Nanoparticle-Mediated Epitaxial Assembly of Colloidal Crystals on Patterned Substrates

Wonmok Lee, Angel Chan, Michael A. Bevan, Jennifer A. Lewis,* and Paul V. Braun*

Department of Materials Science and Engineering, Department of Chemical and Biomolecular Engineering, Beckman Institute for Advanced Science and Technology, and Frederick Seitz Materials Research Laboratory, University of Illinois at Urbana-Champaign, 1304 West Green Street, Urbana, Illinois 61801

Received September 11, 2003. In Final Form: February 4, 2004

We have studied the assembly of 3-D colloidal crystals from binary mixtures of colloidal microspheres and highly charged nanoparticles on flat and epitaxially patterned substrates created by focused ion beam milling. The microspheres were settled onto these substrates from dilute binary mixtures. Laser scanning confocal microscopy was used to directly observe microsphere structural evolution during sedimentation, nanoparticle gelation, and subsequent drying. After microsphere settling, the nanoparticle solution surrounding the colloidal crystal was gelled in situ by introducing ammonia vapor, which increased the pH and enabled drying with minimal microsphere rearrangement. By infilling the dried colloidal crystals with an index-matched fluorescent dye solution, we generated full 3-D reconstructions of their structure including defects as a function of initial suspension composition and pitch of the patterned features. Through proper control over these important parameters, 3-D colloidal crystals were created with low defect densities suitable for use as templates for photonic crystals and photonic band gap materials.

Introduction

Three-dimensional (3-D) colloidal crystals assembled from monodisperse colloidal spheres have generated significant interest because of their potential application as photonic band gap materials,[1,2] chemical sensors,[3−5] optical filters,[2,6,7] and switches.[8,9] These applications often require colloidal crystals with controlled lattice geometry, lattice constant, and low defect density. Several approaches have been developed for assembling 3-D colloidal crystals, including sedimentation,[10−14] dip coating,[15,16] and controlled drying through the use of flow cells.[17,18] Three-dimensional colloidal crystals as large as millimeters across and tens of layers thick have been fabricated. However, their crystallographic orientation is not controlled, they often contain stacking faults, and, upon drying, they are susceptible to crack formation. Because of their fundamental and technological importance, recent efforts have been directed toward the assembly and characterization of large, 3-D colloidal crystals with low defect densities.[16,18−23]

Colloidal epitaxy is a promising route for creating 3-D colloidal crystals with defined structure and orientation. Colloidal templating was first proposed by Dinsmore et al.,[24] who studied interactions between polystyrene microspheres, nonadsorbing polystyrene nanoparticles, and substrates patterned with surface features, such as step edges. They showed that hard-sphere binary mixtures give rise to entropic depletion forces between the colloidal microspheres and substrate surface, which could be used to trap, repel, or guide particle motion depending on the nanoparticle volume fraction, particle size ratio, and patterned feature geometry. van Blaaderan et al.[19] first demonstrated the epitaxial assembly of colloidal crystals via sedimentation of microspheres onto a substrate topographically patterned with a square array of holes.[18,19,21,22] In their work, depletion-induced interactions were not necessary to promote the desired microsphere interactions with the patterned features, as each hole served as a microsphere trap (∼0.6 kT) resulting in creation of a 2-D square microsphere array in the first layer. As subsequent layers formed, microspheres settled onto the interstitial site between four adjacent microspheres (2 × 2 array). In this manner, stacking faults are avoided, and after deposition of a sufficient number of a layers, an fcc crystal is formed.[19]

* To whom correspondence should be addressed. E-mail: pbraun@uiuc.edu; jalewis@uiuc.edu.

(1) Anderson, P. W. *Phys. Rev.* **1958**, *109*, 1492−1505.
(2) Joannopoulos, J. D.; Meade, R. D.; Winn, J. N. *Photonic Crystals: Molding the Flow of Light*; Princeton University Press: Princeton, NJ, 1995.
(3) Holtz, J. H.; Asher, S. A. *Nature* **1997**, *389*, 829−832.
(4) Lee, K.; Asher, S. A. *J. Am. Chem. Soc.* **2000**, *122*, 9534−9537.
(5) Lee, Y.-J.; Braun, P. V. *Adv. Mater.* **2003**, *15*, 563−566.
(6) Yablonovitch, E. *Phys. Rev. Lett.* **1987**, *58*, 2059−2062.
(7) John, S. *Phys. Rev. Lett.* **1987**, *58*, 2486-2489.
(8) John, S. *Phys. Rev. Lett.* **1984**, *53*, 2169−2172.
(9) Pan, G.; Kesavamoorthy, R.; Asher, S. A. *Phys. Rev. Lett.* **1997**, *78*, 3860−3863.
(10) Pusey, P. N.; van Megen, W. *Nature* **1986**, *320*, 340−342.
(11) Pusey, P. N.; van Megen, W.; Bartlett, P.; Ackerson, B. J.; Rarity, J. G.; Underwood, S. M. *Phys. Rev. Lett.* **1989**, *63*, 2753−2756.
(12) Russel, W. B.; Saville, D. A.; Schowalter, W. R. *Colloidal Dispersions*; University Press: Cambridge, UK, 1989.
(13) Davis, K. E.; Russel, W. B.; Glantsching, W. J. *Science* **1989**, *245*, 507−510.
(14) Ackerson, B. J.; Schätzel, K. *Phys. Rev. E* **1995**, *52*, 6448−6460.
(15) Jiang, P.; Ostojic, G. N.; Narat, R.; Mittleman, D. M.; Colvin, V. L. *Adv. Mater.* **2001**, *13*, 389−393.
(16) Vlasov, Y. A.; Bo, X. Z.; Sturm, J. C.; Norris, D. J. *Nature* **2001**, *414*, 289−293.
(17) Park, S. H.; Qin, D.; Xia, Y. *Adv. Mater.* **1998**, *10*, 1028−1031.
(18) Yin, Y.; Xia, Y. *Adv. Mater.* **2002**, *14*, 605−608.
(19) van Blaaderen, A.; Ruel, R.; Wiltzius, P. *Nature* **1997**, *385*, 321−324.
(20) Park, S. H.; Xia, Y. *Adv. Mater.* **1998**, *10*, 1045−1048.
(21) Lin, K. H.; Crocker, J. C.; Prasad, V.; Scohfield, A.; Weitz, D. A.; Lubensky, T. C.; Yodh, A. G. *Phys. Rev. Lett.* **2000**, *85*, 1770−1773.
(22) Braun, P. V.; Zehner, R. W.; White, C. A.; Weldon, M. K.; Kloc, C.; Patel, S. S.; Wiltzius, P. *Adv. Mater.* **2001**, *13*, 721−724.
(23) Griesebock, B.; Egen, M.; Zentel, R. *Chem. Mater.* **2002**, *14*, 4023−4025.
(24) Dinsmore, A. D.; Yodh, A. G.; Pine, D. J. *Nature* **1996**, *383*, 239−242.

10.1021/la035694e CCC: $27.50
Published on Web 04/13/2004

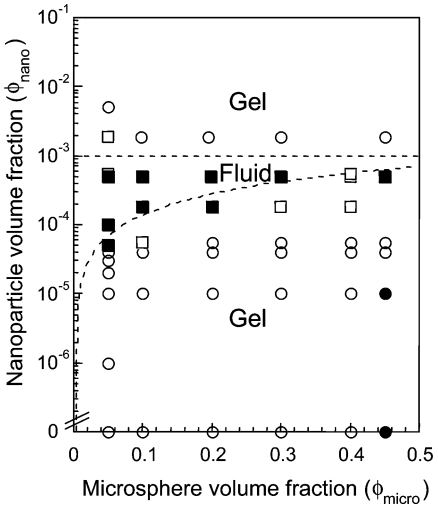

Figure 1. Semilog plot of the phase behavior of microsphere−nanoparticle mixtures of size ratio of 197. Open circles represent a weak colloidal gel and a nanoparticle fluid, filled circles represent a colloidal gel and nanoparticle fluid, filled squares represent a homogeneous fluid (*F*), and open squares represent samples that have separated into a homogeneous fluid and weak gel. The lower and upper dashed lines depict the experimentally observed lower ($\phi^{L,C}$) and upper ($\phi^{U,C}$) critical nanoparticle concentrations, respectively.

The assembly of 3-D colloidal crystals requires colloidal building blocks that are stabilized against flocculation. Colloidal systems that approximate hard-sphere behavior have been utilized in prior studies on colloidal templating.[19,22,24] However, such systems often contain low volatility solvents making drying the colloidal crystal difficult. Alternate routes for stabilizing colloidal building blocks are therefore needed to permit assembly of robust 3-D colloidal crystals that can be successfully dried on corrugated surfaces.

Recently, we reported a new colloidal stabilization mechanism that involves the self-organization of highly charged, hydrous zirconia nanoparticles near the surface of negligibly charged silica microspheres.[25,26] Unlike hard-sphere binary mixtures whose phase behavior is driven solely by entropic effects, energetic considerations must be included in systems that possess both high charge and size asymmetry. We have shown that above a critical nanoparticle concentration, the colloidal microspheres adopt an effective charge that serves to mitigate long-range van der Waals forces providing complete stabilization. By exploiting this novel phase behavior (Figure 1), we have also demonstrated that colloidal crystals could be self-assembled via gravitational sedimentation.[25,26] A unique feature of these wet crystalline structures was that the center-to-center separation distance between microspheres was nearly equivalent to their hard-sphere diameter ($\sim 2a_{micro}$). This is important, because their shrinkage and, thus, crack formation upon drying would be minimal. Another unique feature of this binary system is that the nanoparticle solution forms a gel, even at low nanoparticle volume fractions, when its pH is raised above $\sim$4−6.[27] By gelling the nanoparticle solution surrounding the crystalline sediment, it is expected that a more robust structure could be created that can withstand particle rearrangement and crack formation during drying.

Here, we investigate the epitaxial assembly of 3-D colloidal crystals via sedimentation of dilute binary suspensions on patterned substrates of varying pitch. To our knowledge, this is the first example of the nanoparticle-mediated colloidal assembly that exploits the ability of such species to induce both microsphere stabilization and subsequent gelation. Focused ion beam lithography was utilized to generate epitaxially patterned substrates. Using laser scanning confocal microscopy (LSCM), we have directly observed the assembly of 3-D colloidal crystals and followed their structural evolution through sedimentation, gelation, and drying. By infilling the dried crystals with an index-matched fluorescent dye solution, we have generated a full 3-D reconstruction of their structure including defects (both vacancies and line defects) as a function of varying suspension composition and pitch of the patterned features. Through proper control over these important parameters, 3-D colloidal crystals were created with low defect densities suitable for use as templates for photonic crystals and photonic band gap materials.

Experimental Section

Materials System. Uniform silica microspheres (Geltech, Alachua, FL) served as the large colloidal species. The microspheres have an average radius, a_{micro}, of 0.59 ± 0.01 μm, as determined from quantitive image analysis carried out on SEM photomicrographs (magnification = 15 000×), and a density of 2.25 g/cm^3, as determined by helium pycnometry (Model AccuPyc 1330, Micromeritics Instrument Corp., Norcross, GA). They possess an isoelectric point at pH $\sim$ 2.5 and a zeta potential of approximately 1 mV at pH = 1.5, as determined by microelectrophoresis (Malvern Zetasizer 3000, Malvern Instruments Ltd., Worcestershire, U. K.). The Debye length (κ^{-1}) is 1.8 nm under the experimental conditions of interest (pH = 1.5).

Hydrous zirconia nanoparticles (Zr 10/20, Nyacol Products, Ashland, MA) served as the smaller colloidal species. These nanoparticles have an average radius, a_{nano}, of 3 nm, as determined by X-ray scattering measurements with a reported radius range of 0.5−11 nm.[27] Their reported density is 3.65 g/cm^3.[28,29] They are supplied in an acidic solution (pH = 0.5) at a volumetric solids loading of 7.4%. At pH = 1.5, they possess a zeta potential of 63 ± 12 mV, as determined by microelectrophoresis (Malvern Zetasizer 3000) This value is in reasonable agreement with the zeta potential of $\sim$70 mV estimated from their reported effective charge determined from titration studies[25] using the approach outlined by Gisler et al.[30]

Suspension Preparation. A concentrated binary suspension was prepared by first adding an appropriate volume fraction of silica microspheres ($\phi_{micro} = 0.05$) to deionized water. This stock suspension was stirred for approximately 18 h with three intermittent sonications (Model 550 Sonic Dismembrator, Fisher Scientific, Pittsburgh, PA) during the first 6 h. Nitric acid (reagant grade, Fisher Scientific) was then added to adjust the suspension pH to 1.5 ± 0.1. Each suspension was then sonicated followed by the addition of an appropriate volume fraction of nanoparticles ($\phi_{nano} = 3 \times 10^{-4}$). This composition resided within the homogeneous binary fluid phase, as shown in Figure 1. After stirring several hours, the suspension pH was readjusted to a value of 1.5 (if needed) and sonicated a final time. Each sonication step consisted of 5 min pulsed 1 s on/off sequence at 20 kHz. Aliquots of this binary stock suspension were then diluted by adding an appropriate amount of the nanoparticle solution ($\phi_{nano} \sim 3 \times 10^{-4}$) obtained from the supernatant of a separate stock suspension sedimented under gravity. Two diluted suspensions were prepared with ϕ_{micro} of 10^{-3} and 2.5×10^{-3}, respectively, both with $\phi_{nano} \sim 3 \times 10^{-4}$.

(25) Tohver, V.; Smay, J. E.; Braem, A.; Braun, P. V.; Lewis, J. A. *Proc. Natl. Acad. Sci. U.S.A.* **2001**, *98*, 8950−8954.
(26) Tohver, V.; Chan, A.; Sakurada, O.; Lewis, J. A. *Langmuir* **2001**, *17*, 8414−8421.
(27) Peyre, V.; Spalla, O.; Belloni, L.; Nabavi, M. *J. Colloid Interface Sci.* **1997**, *187*, 184−200.
(28) Miller, K. T.; Zukoski, C. F. *J. Am. Ceram. Soc.* **1994**, *77*, 2473−2478.
(29) Flinkinger, G. L. Thesis, University of Illinois at Urbana-Champaign, Urbana, IL, 1997.
(30) Gisler, T.; Schulz, S. F.; Borkovec, M.; Sticher, H.; Schurtenberger, P.; D'Aguanno, B.; Klein, R. *J. Chem. Phys.* **1994**, *101*, 9924−9936.

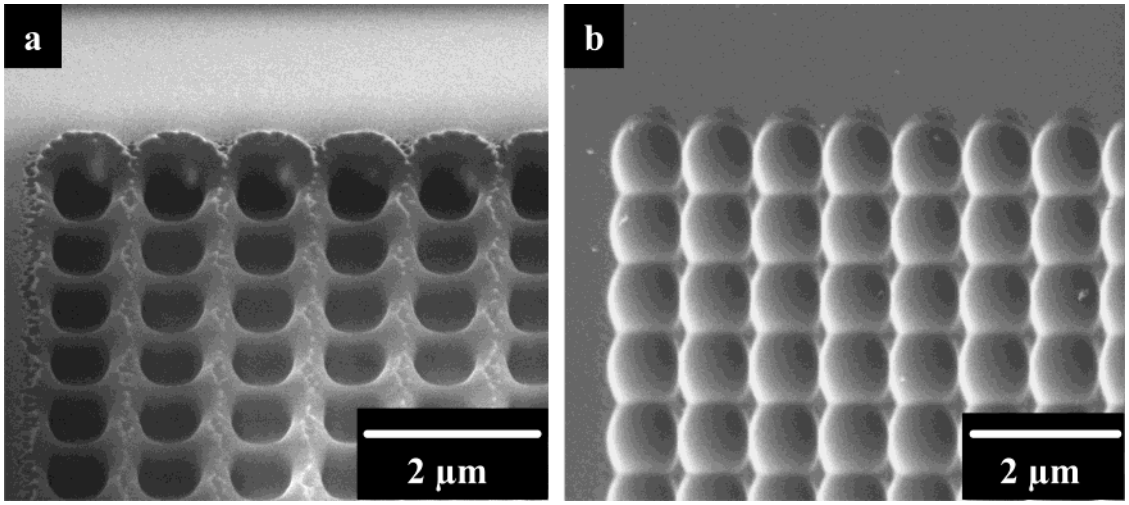

Figure 2. SEM images of the FIB patterned glass substrates. (a) As-milled substrate showing deposited debris around each patterned feature. (b) Cleaned and etched substrate, with a dimple pitch of 1.21 μm and depth of ~400 nm.

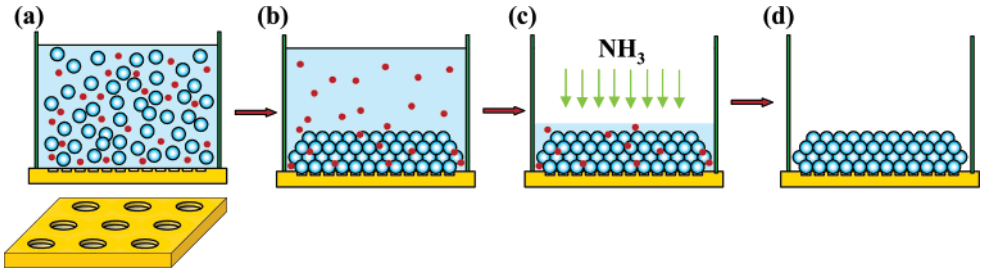

Figure 3. Schematic illustration of the colloidal assembly process: (a) microspheres settling from a dilute binary mixture onto an epitaxially patterned substrate, (b) formation of a 3-D colloidal crystal, (c) removal of excess supernatant solution followed by in situ gelation of the remaining nanoparticle solution through exposure to ammonia vapor, and (d) dried colloidal crystal.

Epitaxially Patterned Substrates. Glass cover slips (18 mm × 18 mm) were sputter coated with 2 nm of Au/Pd and then patterned in a Strata DB-235 dual-beam focused ion beam (FIB) milling system (FEI, Hillsboro, OR). A 40 × 40 square array pattern of circles was drawn as a bitmap and converted to the format used by the FIB system. A square array of 400-nm deep holes of varying pitch was milled into the substrate by a focused Ga ion beam (3000 pA with an aperture size of 100 nm) that was scanned over the substrate surface for 8 min. The center-to-center spacing (pitch) between holes was 1.18 μm, 1.21 μm, or 1.26 μm ± 0.01 μm, which was obtained by varying the magnification of the FIB system. Substrates were produced with either individual patterns or all three patterns on a single surface. The patterned substrates were then sequentially treated with aqua regia (3:1 volume mixture of concentrated nitric acid and hydrochloric acid) to remove the Au/Pd film, 5% aq hydrofluoric acid (HF, Fisher Scientific) for 1 min, Piranha (3:1 volume mixture of concentrated sulfuric acid and hydrogen peroxide, Fisher Scientific), and 1 M aqueous sodium hydroxide (NaOH, Fisher Scientific). The HF etching process removed silica deposited on the substrate during FIB milling and also rounded the patterned features to better accommodate silica microspheres during colloidal epitaxy (see Figure 2).

Colloidal Assembly, Gelation, and Drying. Colloidal silica microspheres suspended in stable, dilute binary fluids underwent gravity-driven sedimentation and crystallization on flat and epitaxially patterned substrates in the custom sample cells illustrated schematically in Figure 3. These cells were fabricated by attaching a glass tube (10 or 25 mm (H) × 8 mm (i.d.)) to each substrate surface using PDMS (Sylgard 184, Dow Corning, Midland, MI). Each sample cell was placed on the confocal microscope stage and leveled prior to introducing either 0.5 mL of binary suspension ($\phi_{micro} = 2.5 \times 10^{-3}$) into the 10-mm high tube or 1.25 mL of binary suspension ($\phi_{micro} = 10^{-3}$) into the 25-mm high tube. This yielded a nominal sediment height of 40 μm. Sedimentation and crystallization were completed in less than 3 h in good agreement with the calculated sedimentation rate of 0.01 mm/s for individual silica microspheres ($a = 0.590$ μm) in water. After 3 h, the supernatant solution was carefully removed from each sample cell. The wet crystalline sediment was then exposed to ammonia vapor for 30 min, which induced gelation of the remaining nanoparticle solution.[27,29] During this process, the pH was raised to ~9.0, which is well above the pH of ~4−6 required for gelation.[29] The sample was then dried under ambient conditions and infilled with a nearly index-matched dimethylformamide (DMF, Fisher Scientific) solution that contained 10^{-4} M Rhodamine 6G (Molecular Probes, Inc., Eugene, OR) fluorescent dye.

Laser Scanning Confocal Imaging. Sample imaging was carried out using a Leica SP-2 equipped with a 63×, 1.32 numerical aperture oil-immersion objective lens (Zeiss, Germany) and a 514-nm laser excitation source. Colloidal microsphere assembly from dilute binary suspensions was monitored using a 633-nm laser scanned across the substrate−suspension interface during sedimentation. Intermittently, after sedimentation, drying, and gelation were completed, real-time LSCM reflection images were acquired both parallel and perpendicular to selected regions on epitaxial- and nonpatterned substrates. Fluorescence imaging of dried, infilled samples was also performed.

Image Analysis. The confocal microscope was calibrated using a calibration grid with a 25-μm mesh size. The pitch of the FIB patterns was determined by measuring from the center of one dimple to the center of another dimple along a line of at least 10 dimples and then dividing by the number of dimples in the line. The error in the measurement is impacted by several factors, including the finite pixel size, determination of feature centers, and drift in the calibration of the confocal microscope. The pixel dimension in the confocal images was ~0.06 μm on a side, and thus an error in the determination of dimple centers by ±2 pixels (normal for our images) results in an error of ±0.12 μm, or ±0.01 μm for the dimple pitch. This error in determining the center of the features can be partially negated by taking multiple measurements. All measurements were performed several times (>4) and were within ±0.01 μm of one another. There is some drift in the calibration of the confocal microscope, but this primarily occurs along the fast scan direction (x-direction). Along

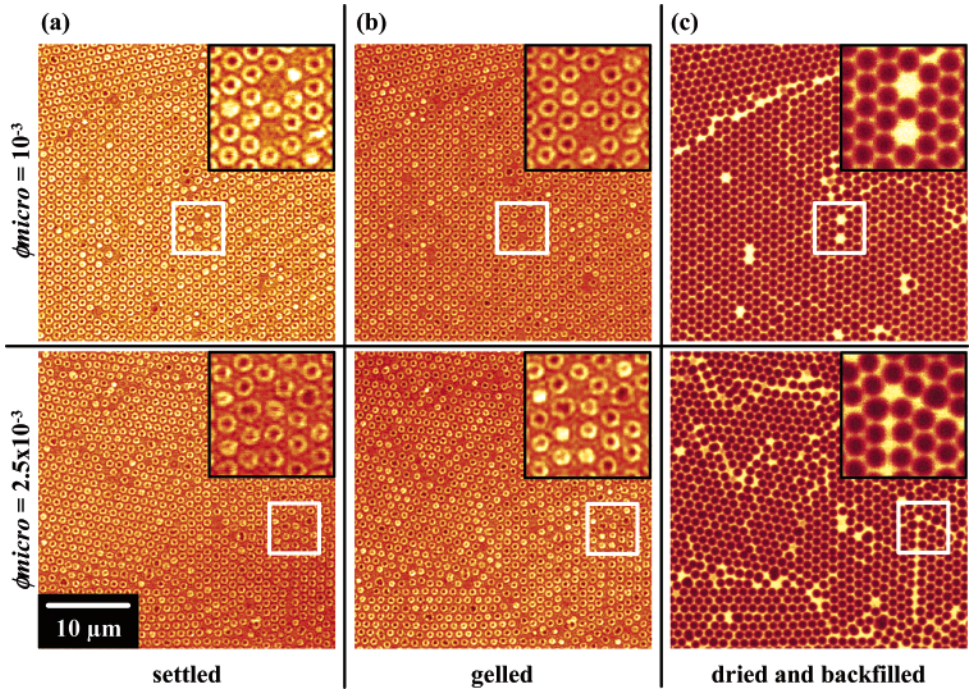

Figure 4. Confocal images ($x-y$ scans of layer one) of colloidal crystals assembled onto a flat substrate from dilute binary suspensions of $\phi_{micro} = 10^{-3}$ (top row) and $\phi_{micro} = 2.5 \times 10^{-3}$ (bottom row): (a) as-settled, (b) gelled, and (c) dried and backfilled with an index-matched, fluorescent dye solution (fluorescence image).

the y-direction, the microscope was stable over days to ±1%. Therefore, we estimate that the dimple pitch error between experiments is about ±0.02 μm.

The center-to-center measurements of the colloidal crystals on flat substrates were determined two different ways. For samples sedimented from binary suspension ($\phi_{micro} = 10^{-3}$), the particle−particle spacing was evaluated by plotting the average two-dimensional number density, $N(r, \theta)$,[31]

$$N(r,\theta) = \langle \rho(n,r,\theta) \rangle_n$$

which is the two-dimensional density around each particle averaged over all particles, and then determining the average spacing over 30 maxima along the y-direction passing through the central spot in the image. $N(r, \theta)$ for the six images presented in Figure 4 are included as Supplementary Information. This analysis was performed using IDL (Research Systems, Inc., Boulder, CO). Intrinsically, this approach is highly accurate, with an error of ±0.12 μm (2 pixels) over 30 maxima, or ±4 nm for the particle−particle spacing. Thus, the calibration of the confocal microscope (±0.01 μm/μm) is the primary source of error using this approach.

For samples sedimented from binary suspension ($\phi_{micro} = 2.5 \times 10^{-3}$), the particle−particle spacing was determined by measuring along a line of at least 10 particles along the y-direction in the images. Determination of the particle centers could be determined ±2 pixels, which adds an error of ±0.01 μm to the determination of particle−particle separation; thus, the total particle−particle separation error in the 0.25 vol % system is ±0.02 μm. Plotting $N(r, \theta)$ to determine the particle−particle spacing was not successful for these images, because they were highly polycrystalline and therefore the average two-dimensional number density plots were nearly featureless away from the central spot.

Results

Colloidal Assembly on Flat Substrates. The first layer of colloidal microspheres sedimented from dilute binary suspensions of varying composition onto a flat substrate is shown in Figure 4. The fully settled structures are depicted for both binary mixtures in Figure 4a. These images reveal that the colloidal microspheres in the first layer have crystallized into a triangular close-packed polycrystalline arrangement with an average center-to-center spacing in the first layer of 1.18 ± 0.01 μm for $\phi_{micro} = 10^{-3}$ and 1.20 ± 0.02 μm for $\phi_{micro} = 2.5 \times 10^{-3}$ determined as described in the experimental procedure. The most important distinction between $\phi_{micro} = 10^{-3}$ and 2.5×10^{-3} was their average domain size, which increased from ~15 μm to ~75 μm in the $x-y$ plane as ϕ_{micro} was reduced from 2.5×10^{-3} to 10^{-3}.

Upon gelling the surrounding nanoparticle solution in the presence of ammonia vapor, these crystalline structures could be frozen in without significant microsphere rearrangement, as shown in Figure 4b. After gelation was completed, the average center-to-center spacing between microspheres for $\phi_{micro} = 10^{-3}$ was 1.19 ±0.01 μm, and 1.20 ±0.02 μm for $\phi_{micro} = 2.5 \times 10^{-3}$. This suggests there is little change in microsphere spacing during the gelation process.

The dried structures were imaged in fluorescent mode through the introduction of an index-matched, fluorescent dye solution, as shown in Figure 4c. These images revealed that there was no further structural rearrangement during drying, which indicated that the "frozen" (gelled) structures were sufficiently robust to prevent reorganization due to capillary stresses. Of equal importance, structures of varying thickness ranging from 20 to 60 μm were successfully dried without crack formation. The average center-to-center separation distance between microspheres for $\phi_{micro} = 10^{-3}$ was 1.20 ±0.01 μm, and 1.20 ±0.02 μm for $\phi_{micro} = 2.5 \times 10^{-3}$, indicating there is little contraction during drying.

Colloidal Assembly on Epitaxially Patterned Substrates. The assembly of colloidal microspheres settled from a dilute binary suspension ($\phi_{micro} = 10^{-3}$; $\phi_{nano} \sim 3 \times 10^{-4}$) onto an epitaxially patterned substrate (1.21-μm pitch) is shown in Figure 5. The plane ($x-y$) and cross-sectional ($x-z$) confocal images of the assembled structure are shown in Figure 5a. By using a relatively long-wavelength 633-nm laser, reflection images were obtained

(31) Loudiyi, K.; Ackerson, B. J. *Physica A* **1992**, *184*.

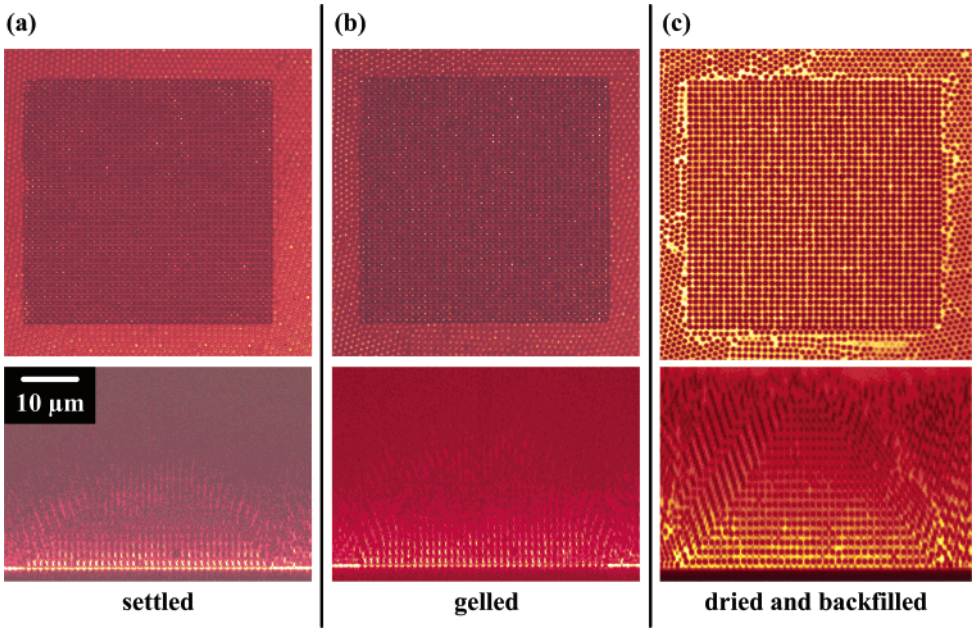

Figure 5. Confocal images ($x-y$ scans of layer one, top row, and $x-z$ scans, bottom row) of a colloidal crystal assembled onto an epitaxially patterned substrate (1.21 μm pitch) from a dilute binary suspension of $\phi_{micro} = 10^{-3}$: (a) as-settled, (b) gelled, and (c) dried and backfilled with an index-matched, fluorescent dye solution (fluorescence image).

through greater than 10 layers of this structure despite significant differences between the refractive index of water and the silica-based microspheres and patterned substrates. Images, acquired for both settled (Figure 5a) and gelled (Figure 5b) structures, indicated the formation of crystallized structure on and above the patterned region of the substrate. Structures assembled onto patterned substrates, in the absence of gelation, could not be successfully dried without disrupting the colloidal crystal. In plane view, there were no apparent microsphere structural transformations observed during nanoparticle gelation. The structural features can be seen more clearly in Figure 5c, which depicts the colloidal crystal after gelation, drying, and subsequent infilling with the index-matched, fluorescent dye solution. In the plane view, each dimpled feature within the patterned region was occupied by a colloidal microsphere (i.e., there were no vacancies). Adjacent to this patterned region, the defect population was substantially higher, as the microspheres again crystallized into a triangular array on the underlying flat surface.

The pyramidal structure adopted by this epitaxially assembled crystal is depicted in the cross-sectional view shown in Figure 5c. It is comprised of 40 layers, where nth layer consists of $(41 - n) \times (41 - n)$ square array of colloidal microspheres and n varies from 1 (sediment−substrate interface) to 40 (top of the pyramid). This structure has evolved on the patterned surface, because only microspheres that settle into the interstitial sites formed by four microspheres (2×2 array) in the underlying layer will crystallize epitaxially. Confocal images of selected layers within this crystal are shown in Figure 6. Point defects present within these layers appear as bright yellow spots. In addition to point defects that diminish in concentration with increasing layer number, there was also evidence of larger defective regions within the pyramidal crystal, which appeared in some, but not all the epitaxially grown crystals. In layer 10, for example, there is a disordered region near the middle of the image comprised of several lattice sites.

The structural evolution of epitaxially assembled colloidal crystals as a function of varying pitch is shown in Figure 7. Plane and cross-sectional confocal images of colloidal crystals formed on a substrate with 1.18-μm, 1.21-μm, and 1.26-μm pitch patterns were acquired after sedimentation, gelation, drying, and infilling with an index-matched, fluorescent dye solution. The sedimentation conditions were identical for all three patterns, as they were adjacent to one another on the same substrate. The plane views of each structure highlight a significant population of point defects in their first layer. The number of missing microspheres in the bottom layer was 90 (out of 1600 sites) for the 1.18 μm, which decreased to 49 and 25 for the 1.21 μm and 1.26 μm patterns, respectively. Line defects were also observed in crystals assembled on these patterned surfaces. The resulting pyramidal colloidal crystals created on each patterned region are shown in the cross-sectional views. These images demonstrate that line defects present in underlying layers propagate deeper into the crystal affecting the structural evolution of subsequent layers. A more detailed description of the effects of binary suspension composition and substrate pitch on defects is provided in the next section.

Complete pyramid formation was not observed in the images shown in Figure 7 because of the low initial volume of binary suspension utilized in that experiment. Layer 31 (10×10 array) was the highest layer that was fully formed in these structures. To demonstrate that this approach is also suitable for thicker sediment structures, epitaxial assembly of a binary suspension ($\phi_{micro} = 2.5 \times 10^{-3}$; $\phi_{nano} \sim 3 \times 10^{-4}$) was carried out on a 1.21 μm pitch substrate with a higher initial suspension volume in the sample cell. The cross-section view of the assembled structure was acquired after sedimentation, gelation, drying, and infilling with an index-matched, fluorescent dye solution, as shown in Figure 8. In this image, one can readily discern the pyramidal colloidal crystal assembled on the epitaxially patterned region of the underlying substrate. In addition, it is evident that the faces of this structure also serve as templates, which guide microsphere crystallization in the regions adjacent to the pyramid. A systematic study of defects in these regions was not carried out. Clearly, the gelled sediment is highly robust, being

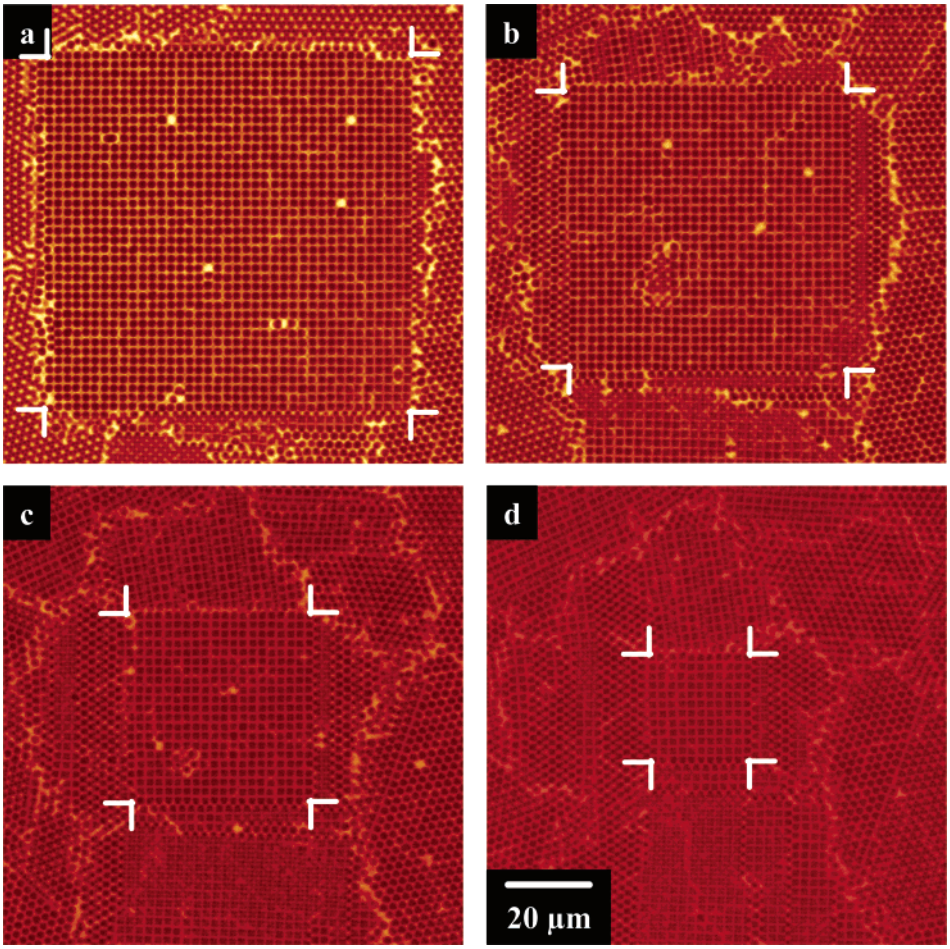

Figure 6. Fluorescence confocal images ($x-y$ scans) of colloidal crystal assembled onto an epitaxially patterned substrate (1.21 μm pitch) from a dilute binary suspension of $\phi_{micro} = 10^{-3}$: (a) layer 2, (b) layer 10, (c) layer 20, (d) layer 30. All micrographs were taken at the same magnification after settling, gelling, drying, and backfilling were completed. The white brackets highlight the region present in each layer affected by the underlying patterned surface.

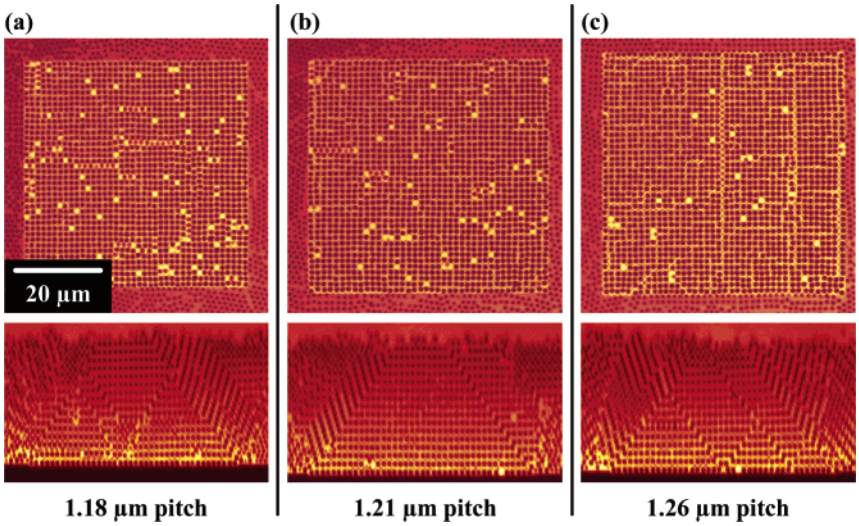

Figure 7. Fluorescence confocal images ($x-y$ scans of layer one, top row, and $x-z$ scans, bottom row) of colloidal crystals assembled onto epitaxially patterned substrates of varying pitch from a dilute binary suspension of $\phi_{micro} = 2.5 \times 10^{-3}$: (a) 1.18 μm pitch, (b) 1.21 μm pitch, (c), 1.26 μm pitch. All micrographs are the same magnification and were collected after settling, gelling, drying, and backfilling were completed.

able to withstand capillary forces during drying without crack formation, even when its thickness exceeds 100 microns.

Compositional and Substrate Effects on Defect Density. The vacancy concentration was determined for colloidal crystals assembled from dilute binary suspensions of varying composition on both flat and epitaxially patterned substrates, as shown in Figure 9. This concentration was defined by the number of vacancies per lattice site in a given layer. On a flat substrate, the vacancy concentration is more difficult to determine because of the presence of domain boundaries; therefore, the defini-

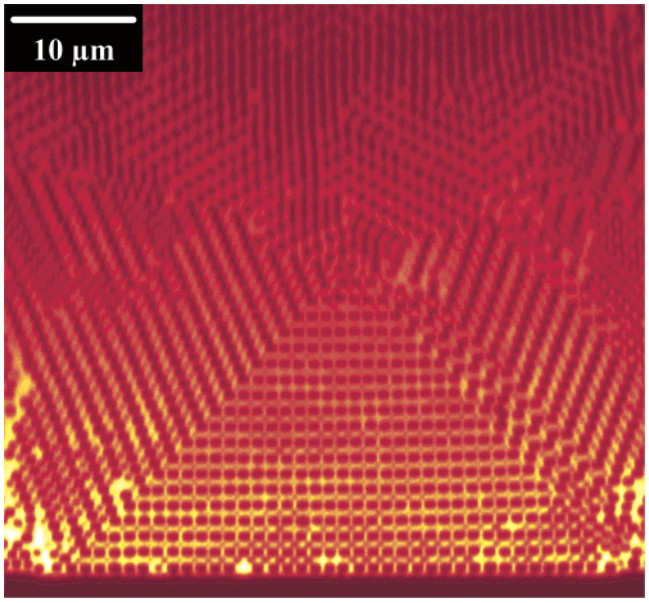

Figure 8. Fluorescence confocal image ($x-z$ scan) of a colloidal crystal assembled onto an epitaxially patterned substrate (1.21 μm pitch) from a binary suspension of $\phi_{\text{micro}} = 2.5 \times 10^{-3}$.

tion applied here was to only count vacancies within individual crystalline domains. Because of wall effects, the first few layers were more defective than subsequent layers, where the vacancy concentration was reduced to ~1−5 vacancies per 1000 lattice sites (see Figure 9a). Near the substrate interface, the vacancy concentration was nearly independent of the initial microsphere volume fraction in suspension. For higher layer numbers (>5), the vacancy concentration was higher for crystals assembled from binary mixtures of higher microsphere volume fraction. There appears to be a linear relationship between these two parameters on the basis of the average values calculated for layers 6−15.

The vacancy concentration of colloidal crystals assembled from a dilute binary suspension ($\phi_{\text{micro}} = 2.5 \times 10^{-3}$) on an epitaxially patterned substrate of varying pitch is shown in Figure 9b. Near the substrate interface, a higher vacancy concentration was observed for each pyramidal crystal. Not surprisingly, the vacancy concentration in the first layer decreased with increasing pitch, as the microspheres could be more easily accommodated on such surfaces. There was a significant decrease in the vacancy concentration between layers 1−3 within each pyramidal crystal, which fell off more gradually in the subsequent layers as the substrate pitch decreased. Beyond layer 10, a vacancy concentration of ~1−5 vacancies per 1000 lattice sites was observed that was nearly independent of substrate pitch.

The vacancy concentration of colloidal crystals assembled from dilute binary suspensions of varying composition on an epitaxially patterned substrate (1.21 μm pitch) is shown in Figure 9c. Interestingly, near the substrate interface, there is a dramatic difference in the vacancy concentration between pyramidal crystals assembled from binary mixtures comprised of $\phi_{\text{micro}} = 10^{-3}$ and 2.5×10^{-3}, with the latter sample possessing at least an order of magnitude higher vacancy concentration in the first layer. This can be observed directly in the plane views of each layer shown in Figure 5c ($\phi_{\text{micro}} = 10^{-3}$) and Figure 7b ($\phi_{\text{micro}} = 2.5 \times 10^{-3}$). Beyond the first few layers, however, there was little difference between the two systems, and their vacancy concentration was ~1−5 per 1000 microspheres.

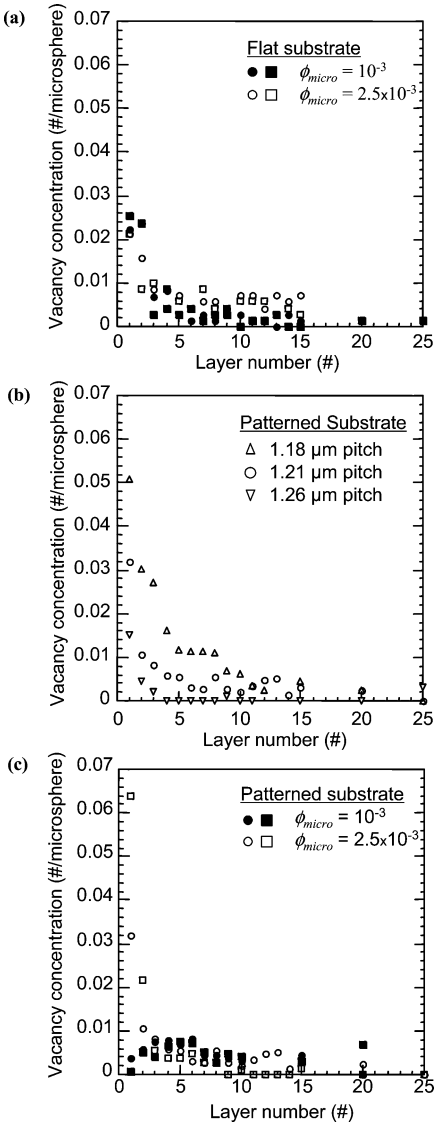

Figure 9. Plots of vacancy concentration (fraction of missing microspheres per microsphere in a given layer) as a function of layer number within colloidal crystals assembled onto flat and epitaxially patterned substrates from dilute binary mixtures of varying microsphere volume fraction: (a) $\phi_{\text{micro}} = 10^{-3}$ and 2.5×10^{-3}, flat substrate, (b) $\phi_{\text{micro}} = 2.5 \times 10^{-3}$, patterned substrates of varying pitch, and (c) $\phi_{\text{micro}} = 10^{-3}$ and 2.5×10^{-3}, patterned substrate, 1.21 μm pitch.

Line defects were the other predominant feature observed in the epitaxially assembled colloidal crystals, as shown in Figure 7. The cross-sectional images reveal their presence, especially in crystals assembled on 1.18 μm and 1.26 μm pitch patterned regions. The patterned region with the finest pitch cannot easily accommodate a square-packed array of microspheres. Line defects appear to form when the microspheres locally pack in a triangular array, that is, when they are pushed close together. In contrast, the patterned region with the largest pitch can too easily accommodate a square-packed array of microspheres, and dislocations result when an additional line of microspheres are inserted from above into the square lattice within a given layer. The cross-sectional images in Figure 7 show the propagation of these defects into the upper layers of the pyramidal colloidal crystal. Such defects create triangular wedge-shaped regions within the crystal, which are shifted up or down by some fraction of a lattice constant. For crystals epitaxially

assembled on the 1.21 μm pitch patterned region, few line defects were observed.

Discussion

Nanoparticle-Mediated Colloidal Assembly. Our assembly route exploits the ability of hydrous zirconia nanoparticle species to induce both microsphere stabilization and subsequent gelation. The use of highly charged nanoparticles to stabilize colloidal microspheres by regulating their effective charge contrasts greatly with the traditional approach of tailoring solution pH well away from the isoelectric point. We have previously shown that these binary mixtures are fully stabilized when the nanoparticle volume fraction lies within the critical concentration range of $\phi^{L,C} \leq \phi_{nano} < \phi^{U,C}$, where $\phi^{L,C}$ denotes the transition from the lower gel region to homogeneous binary fluid phase induced by nanoparticle stabilization and $\phi^{U,C}$ denotes the transition from the homogeneous binary fluid phase to the upper gel region because of depletion forces (see Figure 1).

Here, we have demonstrated that nanoparticle stabilization mediates colloidal assembly on epitaxially patterned substrates in two important ways. First, this stabilization mechanism allows the colloidal microspheres to assemble into a nearly touching network, as evidenced by their minimum separation distance on flat substrates of less than 2% of their hard-sphere diameter ($D \sim 1.18$ μm). This value is significantly lower than that reported for the identical microspheres stabilized via charge stabilization in the absence of nanoparticle additions, where the minimum separation distance was approximately 7% of their hard-sphere diameter.[26] Nanoparticle stabilization is therefore advantageous as it allows the formation of a crystalline structure that experiences minimal shrinkage during drying. Second, the use of hydrous zirconia nanoparticles permits the subsequent gelation of this structure yielding a robust colloidal assembly that can withstand capillary drying stresses without cracking.

The phase behavior, structure, and rheology of hydrous zirconia nanoparticle solutions, identical to those utilized here, have been investigated previously by Peyre et al.[27] and Flinkinger.[29] The nanoparticles are highly charged ($\zeta \sim 60$ mV) under low pH conditions. Their surface charge is balanced by NO_3^- counterions in solution. In addition to nanoparticles, Peyre et al.[27] also report the presence of other zirconium (e.g., tetrameric ions, $[Zr(OH)_2(OH_2)_4]_4^{8+}$) or zirconium−nitrate species in solution, which can be removed by dialysis. Zirconium chemistry is notoriously complex, and thus the precise identity of these species is not known.[27] Flinkinger[29] has previously reported that hydrous zirconia nanoparticles undergo polymerization and hydrolysis when the solution pH is raised above ~4−6. Interestingly, chemical gelation occurs in this system at low nanoparticle volume fractions (i.e., about 10^{-3}). The gel-like structure is maintained when diluted under these conditions; however, this transition is fully reversible upon lowering pH. We have exploited this unique chemistry to induce gelation of the dilute nanoparticle solution that surrounds the colloidal microspheres within the crystallized sediment. After gelation, this structure can be successfully dried without cracking. Because of the close-packed nature of the colloidal microspheres, little shrinkage was observed during the gelation and drying process.

Compositional Effects on Colloidal Epitaxy. The epitaxial assembly of colloidal crystals via sedimentation of colloidal microspheres onto patterned substrates involves a complex interplay of gravitational settling, diffusion, and crystallization. Because the volume fraction where crystallization occurs is constant, this process is governed by the maximum crystallization rate ($\sim kT/a^2$), the sedimentation rate ($\sim \Delta\rho g a^2$), and the initial ϕ_o.[12,32,33] For the dilute binary suspensions studied here, the rate of crystal growth is uniquely determined by their initial microsphere volume fraction (ϕ_{micro}).[32] This situation arises because the microsphere flux from the free settling region to the region above the sediment (known as the fan) is less than the maximum possible flux ($\phi^* U(\phi)$), where ϕ is the local volume fraction of particles in the fan and $U(\phi)$ is the sediment velocity given by[12,32]

$$U(\phi) = \frac{2}{9}\left(\frac{a^2 \Delta\rho g}{\nu}\right)(1-\phi)^{6.6}$$

van Blaaderan and co-workers[32] defined the following system parameter, $(\phi_o Pe)^{-1}$, which is equivalent to the ratio of $t_{sed}/t_{diffusion}$, where t_{sed} and $t_{diffusion}$ correspond to the characteristic sedimentation and diffusion times, respectively. For initial microsphere volume fractions of 10^{-3} and 2.5×10^{-3}, $(\phi_o Pe)^{-1}$ is equal to 667 and 267, respectively, where Pe ($=4/3\pi a^4 \Delta\rho g/kT$) equals 1.5 for both dilute binary suspensions. These values indicate that the characteristic sedimentation time far exceeds the diffusion time, such that microspheres have an opportunity to assemble into the observed crystalline sediments in both cases.

On patterned substrates, there were significant compositional effects on crystallization near the substrate−sediment interface. For example, the vacancy concentration measured for colloidal crystals epitaxially assembled from a dilute binary suspension of $\phi_{micro} = 2.5 \times 10^{-3}$ was nearly an order of magnitude higher in the first layer relative to that observed for the analogous crystal assembled at $\phi_{micro} = 10^{-3}$ (Figure 9c). The diffusivity of colloidal microspheres on a patterned surface is likely to be significantly lower than $t_{diffusion}$, because particles can become "trapped" in the dimpled regions thereby suppressing their characteristic diffusion time. van Blaaderan and co-workers[32] recently reported that even on a flat substrate, the equilibration time is less than that found for higher layers within the sediment. They have shown that this difference manifests itself as an increase in the number of stacking faults within layers 1−3 when colloidal assembly is carried out on a flat substrate.[32] On patterned substrates, this difference is reflected in a higher population of point defects within these layers. In sharp contrast, colloidal crystals assembled from these same binary systems on a flat substrate exhibited little difference in their vacancy concentration near the substrate−sediment interface with increasing initial microsphere volume fraction (Figure 9a). Such observations likely stem from differences in the characteristic diffusion times on flat versus patterned surfaces. However, since the vacancy concentration is not a strong function of microsphere concentration in subsequent layers, the observed vacancies may not solely be due to kinetic trapping. Such defects could also arise from polydispersity effects, in which larger microspheres are not easily accommodated by the cavities present in underlying layers.

Beyond the first few layers, the vacancy concentration was essentially independent of the initial microsphere volume fraction for crystals assembled from these dilute

(32) Hoogenboom, J. P.; Derks, D.; Vergeer, P.; van Blaaderen, A. *J. Chem. Phys.* **2002**, *117*, 11320−11328.
(33) Hoogenboom, J. P.; van Langen-Suurling, A. K.; Romijin, J.; van Blaaderen, A. *Phys. Rev. Lett.* **2003**, *90*, 138301.

systems. Their observed concentrations ranged from ~1−5 vacancies per 1000 lattice sites for colloidal crystals formed by sedimentation on either patterned and flat substrates. These values are higher than the theoretical values reported for hard-sphere systems (i.e., ~1 or less vacancy per 4000 lattice sites),[34,35] but far below the defect densities reported by Vlasov et al.[16] for sedimented opals (i.e., ~1 vacancy per 100 lattice sites).

Substrate Pitch Effects on Colloidal Epitaxy. Focused ion beam milling was utilized to create epitaxially patterned substrates. This facile approach provides the ability to rapidly alter patterns without the need for photomasks, such that the effects of a wide range of parameters (e.g., substrate pitch, geometry, depth, and array size) on colloidal crystallization can be assessed. We confined the present study to probe the effects of substrate pitch over the narrow range, that is, D_{c-c}/D_{micro} from ~0.98 to 1.05, assuming a value of D_{micro} of 1.20 μm (i.e., the center-to-center separation distance between microspheres in the dried sediment). Our experimental observations indicate that the exact pitch of the patterned features on the substrate had a significant effect on the quality of the epitaxially assembled colloidal crystal, even over this narrow range (Figure 7). The defects observed for crystals assembled on the 1.18 μm pitch substrate stem from overcrowding phenomena that occurs in the first layer. This occurs when microspheres, whose effective diameter exceeds the center-to-center separation distance of 1.18 μm, attempt to pack adjacent to one another. Both point and line defects were incorporated into this structure as crystallization proceeded. In contrast, line defects were the dominate defect observed for colloidal crystals assembled on the 1.26 μm pitch substrate. In this case, the substrate pitch is ~7% greater than the microsphere diameter, thus it may be possible for the pressure of the overlying layers to insert a partial line of microspheres into the underlying layers. The patterned region that was ~20 nm greater than the center-to-center separation distance between microspheres in the wet, gelled, and dried structures yielded templated crystals with the lowest defect density.

(34) Bennett, C. H.; Alder, B. J. *J. Chem. Phys.* **1971**, *54*, 4796−4808.

(35) Pronk, S.; Frenker, D. *J. Phys. Chem. B* **2001**, *105*, 6722−6727.

Conclusions

We have demonstrated the epitaxial assembly of colloidal crystals via sedimentation of dilute binary mixtures of colloidal microspheres and highly charged nanoparticles on patterned substrates. Nanoparticle species mediated colloidal assembly through a combination of stabilization and subsequent gelation. Nanoparticle stabilization of colloidal microspheres offered superior control over their center-to-center separation distance in the wet crystalline sediments, while their gelation yielded robust structures that could be dried without particle reorganization or cracking. Through analysis of LSCM images of wet and dried colloidal crystals, we found that both the initial microsphere concentration in suspension and the pitch of the substrate pattern were critical to assembling low defect density colloidal crystals. When properly grown, colloidal crystals could be created with defect densities suitable for consideration as templates for photonic band gap materials.

Acknowledgment. This material is based upon work supported in part by the U.S. Department of Energy, Division of Materials Sciences under Award No. DEFG02-91ER45439, through the Frederick Seitz Materials Research Laboratory, and the Beckman Institute, both at the University of Illinois at Urbana-Champaign as well as the National Science Foundation (NSF Grant # DMR-00-71645). Research for this publication was carried out in part in the Center for Microanalysis of Materials, University of Illinois at Urbana-Champaign, which is partially supported by the U.S. Department of Energy under grant DEFG02-91-ER45439. M.A.B. acknowledges support through the Beckman Fellows program at the Beckman Institute, UIUC. We would like to thank J. van Fleet and P. Wiltzius for assistance with IDL.

Supporting Information Available: Images of the average two-dimensional number density, $N(r, \theta)$, for the six images presented in Figure 4 are presented as Supporting Figure 1. LSCM images of layers 1−16, 20, 25, 30, and 35 of the dried and backfilled colloidal crystal formed on a substrate of pitch 1.21 μm are presented as Supporting Figure 2. This material is available free of charge via the Internet at http://pubs.acs.org.

LA035694E